Experimental tuning of transport regimes in hyperuniform disordered photonic materials — Supplemental Material —

Geoffroy J. Aubry,[1,2,*] Luis S. Froufe-Pérez,[1] Ulrich Kuhl,[2] Olivier Legrand,[2] Frank Scheffold,[1] and Fabrice Mortessagne[2]

[1] *Département de Physique, Université de Fribourg, Switzerland*
[2] *Institut de Physique de Nice, Université Côte d'Azur/CNRS, France*

This document contains the scattering properties of a single rod, details on the structures of the point patterns, the band structure calculation, details on the time domain propagation videos and all the technical information on the data analysis. The seven videos show how the electromagnetic wave propagates in the cavity for different frequency ranges (see Supplemental Material Fig. S6 for the description of the videos).

CONTENTS

I. BOLTZMANN SCATTERING MEAN FREE PATH.

In Fig. S1 we show the scattering efficiency Q of an individual cylinder in TM polarization calculated using Mie theory [1] (upper panel). In the lower panel, we show how the corresponding Boltzmann scattering mean free path $\ell_{\rm sca}(\nu) = [\sigma_{\rm sca}(\nu)\rho]^{-1}$ (with $\sigma_{\rm sca}(\nu) = 2rQ_{\rm sca}$ the total scattering cross section) compares with L, the size of the system, and λ_0, the wavelength in vacuum of the wave.

II. POINT PATTERNS AND THEIR STRUCTURE FACTORS.

Figure S2(a) shows the point patterns of the samples studied in this study, and Fig. S2(b) the corresponding

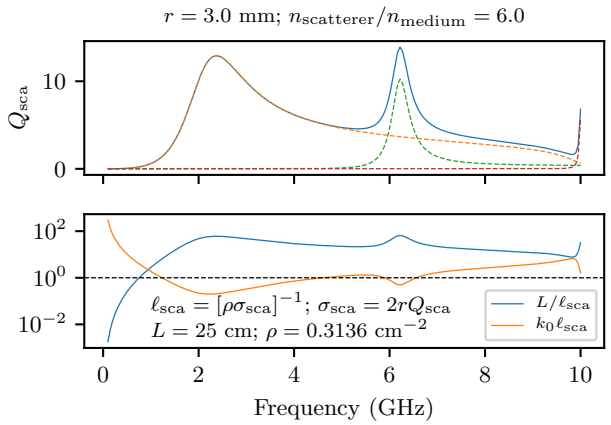

Figure S1. Upper panel: Scattering efficiency $Q_{\rm sca}$ of individual cylinders in TM polarization (solid blue line), and the three first terms in the Mie expansion (dashed lines). Lower panel: optical density $L/\ell_{\rm s}$ in the independent scattering approximation using the Boltzmann scattering mean free path and the sample size L. Also shown is $k_0\ell_{\rm s}$ with $k_0 = 2\pi/\lambda$ and the wavelength in vacuum λ_0 ($k_0 = 2\pi/\lambda_0$).

average structure factors

$$S(\mathbf{k}) = \frac{1}{N}\sum_{j=1}^{N}\sum_{l=1}^{N} \mathrm{e}^{-i\mathbf{k}\cdot(\mathbf{R}_j - \mathbf{R}_l)}, \qquad \text{(S1)}$$

over 1000 samples generated as the ones used in this study, where R_j are the positions of the N points, and $\mathbf{k}$ is the wavevector.

III. VISUALIZATION OF THE EIGENMODES OF THE DISORDERED CAVITY

A. Clustering of the resonances into modes

The measured spectra consist of a superposition of peaks (see Main text Fig. 1(b)) which are associated to

* geoffroy.aubry@unifr.ch

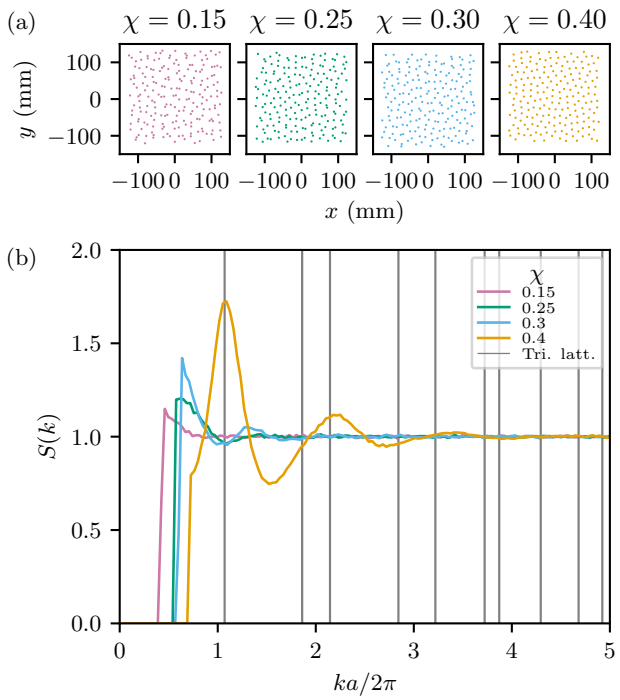

Figure S2. (a) Point patterns of the studied samples. (b) Radially averaged structure factors $S(k)$ of the studied samples as a function of ka, where $a = 1/\sqrt{\rho}$ and ρ denotes the number density of scatterers. The structure factors are averaged over 1000 different realizations of about 200 points. The grey vertical lines indicate the peaks of the radially averaged triangular lattice structure factor (Bragg peaks).

the resonances of the system. We determine the frequencies ν^i, widths γ^i and complex amplitudes A^i of each resonance $i = 1, \ldots, N$ using the harmonic inversion method described in ref. [2, 3]. Ideally, resonances belonging to the same mode should all have the same frequency. In practice, the presence of the mobile antenna at every point (x, y) shifts the resonant frequency by a small amount depending on the intensity of the electromagnetic field at the specific mobile antenna position [4], see Fig. S3. Note that we minimize this perturbation due to the mobile antenna by having it extending into the cavity by only 1 mm whereas the height of the cavity is 5 mm. This has the consequence that it is weakly coupled to the field, and explains the low transmission values as seen in Main text Fig. 1(b). We identify all data points belonging to a certain cluster by using a density-based clustering algorithm [5] fulfilling the condition that two points having the same coordinate (x, y) cannot be in the same cluster. To associate each resonant signal at position (x, y) to a specific mode, we apply a semi-supervised clustering algorithm. This allows us to identify every single mode of the disordered cavity, associated with discrete resonance frequencies, as long as the mode amplitude is large enough to be detected by the vector network analyzer [5, 6].

More precisely, we use a slightly modified version of the C-DBSCAN algorithm published in Ref. [5]. In our version, step 2 of the algorithm [5] either labels the points in the KD-tree leaf as noise ratio (if the density is too small), or we create a local cluster for each point in the leaf. Depending on the frequency range, we run our modified version of C-DBSCAN either in the (x, y, ν), (x, y, ν, γ) or $(x, y, \nu, \gamma, \ln A)$ space to reach the best clustering results. An example of the result is shown in Fig. S3 where the different clusters, or modes, found by the algorithm are plotted using different colors.

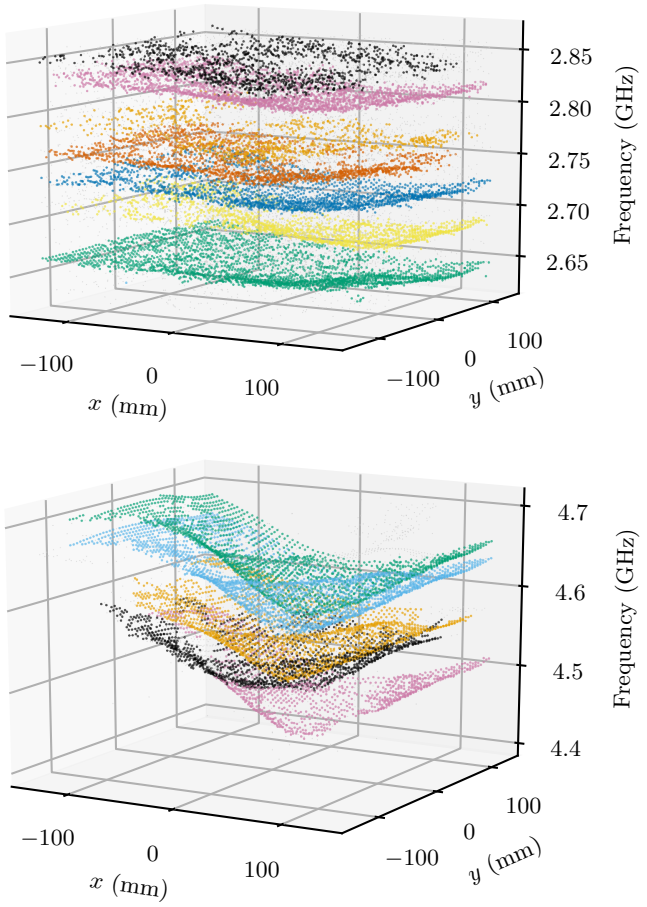

Figure S3. For each position (x, y), a spectrum is measured and the frequencies are extracted using harmonic inversion: these are the points plotted in this figure for two different frequency ranges. The points are then clusterized: each color corresponds to a cluster found by the algorithm. The upper panel corresponds to a typical situation in the stealth regime where the intensity is almost uniform over the sample (small frequency shifts). The lower panel corresponds to the case of localized modes with large intensities corresponding to large frequency shifts.

B. Electric field amplitude maps

In the first line of Main text Fig. 3, we plot the signed amplitude $E_\nu^{\pm}(x,y) = \mathrm{sgn}\left(\mathrm{Re}[\tilde{S}_{12}]\right)|\tilde{S}_{12}|$, where $\tilde{S}_{12}$ is the transmission deduced from S_{12} after the ad hoc rotation of the global phase making the real and imaginary parts statistically independent [7]. This allows to represent both the real and imaginary parts of the eigenmodes on the same map.

IV. NUMERICAL SIMULATIONS OF THE DOS

Figure S4 shows the normalized density of states (nDOS) of the stealthy hyperuniform samples obtained numerically for a large statistical ensemble of point patterns and using periodic boundary conditions. The properties of the dielectric cylinders and their density are identical to those of the system studied in the experiment. The nDOS was calculated using the MIT Photonic Bands [8] software using the supercell method [9] as described earlier in ref. [10]. This dataset was obtained by calculating 500 different samples for each χ-value (between 0.1 and 0.5, every 0.05).

Figure S5 shows the average and the standard deviation of the gap central frequency and width found for the samples used in Fig. S4. The statistical variations are large at low and intermediate χ-values (between 0.10 and 0.35). At large χ-values (≥ 0.4), the standard deviation vanishes: the gap central frequencies and widths are similar from sample to sample.

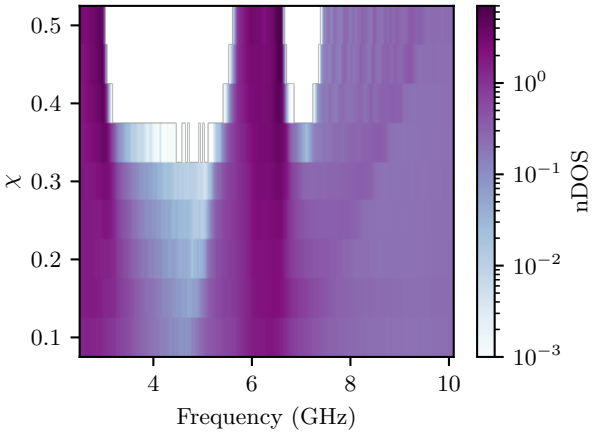

Figure S4. Normalized density of states (nDOS) obtained by taking the average over the band structure calculated numerically for 500 system realizations at each value of χ.

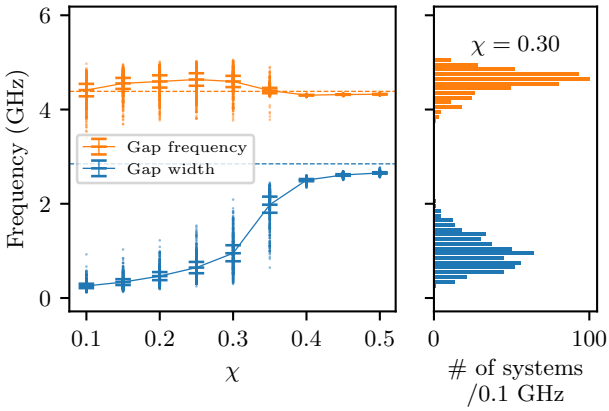

Figure S5. Spread of the first gap central frequency and width found in the numerical results used to obtain Fig. S4. The error bars correspond to the standard deviations, the scattered points to the 500 individual systems per χ-value used to compute the statistics. The dashed lines correspond to the results obtained for the triangular lattice. The right panel shows the histograms for the $\chi = 0.30$ samples.

V. TIME DOMAIN PROPAGATION VIDEOS

We obtain time domain propagation signals from the real part of the Fourier transform of the complex transmission spectra multiplied by a chosen bandpass filter centered at f_0 with a standard deviation $\Delta\nu$. We use a Gaussian bandpass filter to avoid window effects in the Fourier transform. The excitation in the time domain is therefore a Gaussian pulse with a temporal spread inversely proportional to $1/\Delta\nu$ of the Gaussian bandpass filter.

Videos S6-1, 2 and 3 show the propagation of the wave in the low frequency regime (well below the gap frequency $\nu_G \simeq 5$ GHz. We observe that for frequencies $\nu < \nu_c$ and at early times, the spherical wave structure is well preserved, indicating the absence of scattering. This boundary between the stealth regime and the diffusive regime is also shown in more detail in Fig. S7. The panels in the green shaded polygon indicate that the Gaussian pulse central frequency f_0 is below the critical stealth frequency $\nu_c = \frac{c}{n_{\text{eff}}}\sqrt{\frac{pX}{\pi}}$, and above ν_c elsewhere. By eye, we see a clear correlation between the wave front smoothness and the transition from the stealth regime to the diffusive regime for frequencies $\nu > \nu_c$. Since $\nu_c \propto \sqrt{\chi}$ the transition is shifted to higher frequencies when increasing the degree of stealthiness χ. Note that the wave distortion at later times (in the videos) is explained by reflections of the wave on the non-ideal absorbing foam walls.

Video S6-4 (respectively S6-6) shows the electromagnetic field for a Gaussian pulse centered 0.25 GHz below (resp. above) the band gap and having a width $\Delta\nu = 0.25$ GHz. Video S6-7 shows the propagation of the wave in the high frequency regime, well above the first band gap. As in the low frequency regime for frequencies above ν_c, we observe a strong scattering and wave diffusion.

Finally, video S6-5 shows the electromagnetic field in the band gap. For this video, the bandpass filter was chosen to be a square filter fitting exactly the bandgaps as extracted from Main text Fig. 2. This explains the windowing effect seen in the input signal.

[1] C. F. Bohren and D. R. Huffman, *Absorption and Scattering of Light by Small Particles* (Wiley, New York, 1998).

[2] J. Main, P. A. Dando, D. Belkic, and H. S. Taylor, Decimation and harmonic inversion of periodic orbit signals, Journal of Physics A: Mathematical and General **33**, 1247 (2000).

[3] J. Wiersig and J. Main, Fractal Weyl law for chaotic microcavities: Fresnel's laws imply multifractal scattering, Phys. Rev. E **77**, 036205 (2008).

[4] L. C. Maier and J. C. Slater, Field strength measurements in resonant cavities, Journal of Applied Physics **23**, 68 (1952).

[5] C. Ruiz, M. Spiliopoulou, and E. Menasalvas, C-DBSCAN: Density-based clustering with constraints, in *Rough Sets, Fuzzy Sets, Data Mining and Granular Computing*, edited by A. An, J. Stefanowski, S. Ramanna, C. J. Butz, W. Pedrycz, and G. Wang (Springer Berlin Heidelberg, Berlin, Heidelberg, 2007) pp. 216–223.

[6] M. Pourrajabi, D. Moulavi, R. J. G. B. Campello, A. Zimek, J. Sander, and R. Goebel, Model selection for semi-supervised clustering, in *Advances in Database Technology - EDBT 2014*, edited by S. Amer-Yahia, V. Christophides, A. Kementsietsidis, M. Garofalakis, S. Idreos, and V. Leroy (OpenProceedings.org, Konstanz, 2014) pp. 331–342.

[7] O. Xeridat, C. Poli, O. Legrand, F. Mortessagne, and P. Sebbah, Quasimodes of a chaotic elastic cavity with increasing local losses, Phys. Rev. E **80**, 035201(R) (2009).

[8] S. G. Johnson and J. D. Joannopoulos, Block-iterative frequency-domain methods for Maxwell's equations in a planewave basis, Opt. Express **8**, 173 (2001).

[9] J. Joannopoulos, S. Johnson, J. Winn, and R. Meade, *Photonic Crystals: Molding the Flow of Light*, 2nd ed. (Princeton University Press, 2008).

[10] L. S. Froufe-Pérez, M. Engel, P. F. Damasceno, N. Muller, J. Haberko, S. C. Glotzer, and F. Scheffold, Role of short-range order and hyperuniformity in the formation of band gaps in disordered photonic materials, Phys. Rev. Lett. **117**, 053902 (2016).

1. Stealth regime (Gaussian bandpass filter, $f_0 = 1.75$ GHz, $\Delta\nu = 0.25$ GHz)
2. Stealth regime (Gaussian bandpass filter, $f_0 = 2.25$ GHz, $\Delta\nu = 0.25$ GHz)
3. Wave diffusion (Gaussian bandpass filter, $f_0 = 3.5$ GHz, $\Delta\nu = 0.25$ GHz)
4. Dielectric Anderson localized modes just below the bandgap (Gaussian bandpass filter, $\Delta\nu = 0.25$ GHz)
5. Square filter in the bandgaps
6. Air Anderson localized modes just above the bandgap (Gaussian bandpass filter, $\Delta\nu = 0.25$ GHz)
7. Wave diffusion (Gaussian bandpass filter, $f_0 = 6.5$ GHz, $\Delta\nu = 0.25$ GHz)

Figure S6. Videos description. The videos are permanently stored on the Zenodo repository: `https://doi.org/10.5281/zenodo.3978032`.

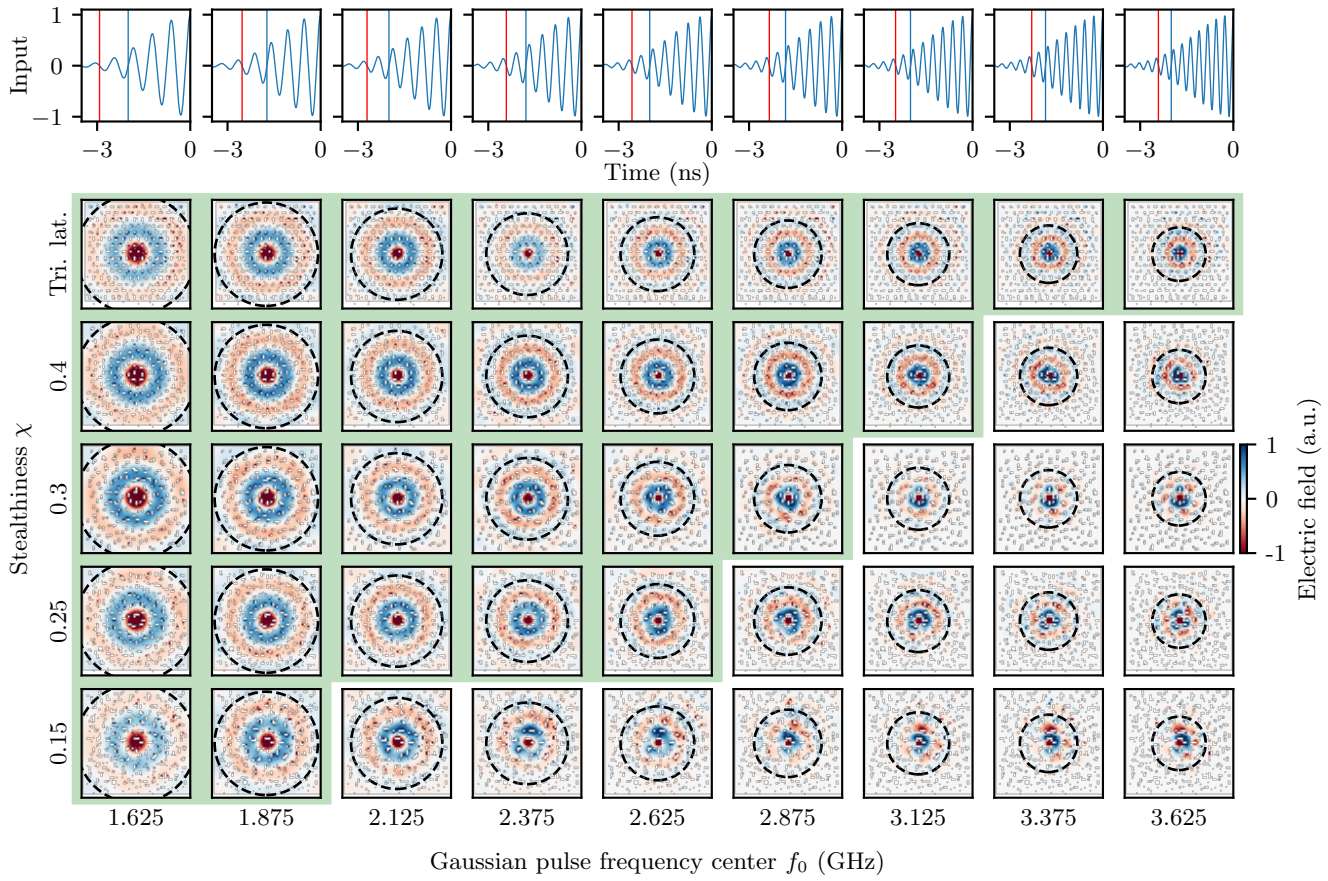

Figure S7. Maps of the electric field amplitude for the propagation of a pulse of spectral width $\Delta\nu = 0.125$ GHz at different central frequencies f_0 (for details see text and Main text Fig. 3, and first half of the Gaussian pulse used for the excitation. The frames shown in the figure are taken at the time marked by the blue vertical line. The panels in the green polygon indicate frequencies below $\nu_c(\chi)$. The radius of the dashed circles indicate the place where a wave emitted at the time marked by the red vertical line should be at the time marked by the blue vertical line, for a homogeneous medium with $n_{\text{eff}} = 1.8$. The color scale is adjusted for each individual panels.